Force-dependent ligand sensing enables αVβ3 integrin to differentiate between fibronectin and high-affinity ligands

Michael Bachmann[1,*], Markus Schäfer[1,2,*], Kai Weißenbruch[1], Vasyl Mykuliak[3], Lia Heiser[1], Clemens M. Franz[4], Vesa Hytönen[3], Bernhard Wehrle-Haller[5,6], Martin Bastmeyer[1,2,6]

Affiliations:
1: Zoological Institute, Cell- and Neurobiology, Karlsruhe Institute of Technology (KIT), Karlsruhe, Germany
2: Institute of Functional Interfaces (IFG), Karlsruhe Institute of Technology (KIT), Karlsruhe, Germany
3: Faculty of Medicine and Life Sciences and BioMediTech, University of Tampere, Finland and Fimlab Laboratories, Tampere, Finland
4: DFG–Center for Functional Nanostructures, Karlsruhe Institute of Technology (KIT), Karlsruhe, Germany
5: Department of Cell Physiology and Metabolism, University of Geneva, Geneva, Switzerland
6: Correspondence should be addressed to B. Wehrle-Haller (Bernhard.Wehrle-Haller@unige.ch) or M. Bastmeyer (martin.bastmeyer@kit.edu).
*: These authors contributed equally.

Abstract:

Integrins sense chemical and mechanical properties of the extracellular matrix (ECM) with some integrins recognizing multiple ECM-proteins. αVβ3 integrin is a receptor for vitronectin (Vn), osteopontin (Opn), fibrinogen (Fbg), and fibronectin (Fn), but the biological consequences of different interactions are poorly understood. Here, we employ binary choice substrates of these proteins to dissect the ligand binding of αVβ3 on the subcellular scale. Super-resolution live cell imaging revealed that αVβ3-mediated adhesion on Fn/Vn substrates exclusively initiate on Vn. Biochemical binding assays and binary choice substrates confirmed higher affinity of αVβ3 for Vn, Opn, and Fbg, compared to Fn. We show that localization of αVβ3-adhesions on Fn is a force-dependent process coupled to hybrid domain swing-out in the β3 headpiece. Vn in contrast is recognized under low mechanical load, enabling αVβ3 to differentiate ligands depending on force. Vn-preference of αVβ3 is preserved on softer substrates, while mechanosensing is determined by inside-out signaling.

Keywords:
Integrin, ECM, integrin affinity, outside-in signaling, mechanotransduction

Introduction:
Integrins, an important class of cell-matrix adhesion receptors, consist of an α- and a β-subunit forming transmembrane heterodimers[1]. While the extracellular part binds to proteins of the extracellular matrix (ECM), the intracellular part is connected to actin via multiple adapter and signaling proteins that make up the so-called adhesome[2, 3]. Integrin activation on the functional level describes the capacity to bind ligands, while on the structural level activation is associated with conformational changes from a bent, to an extended-closed, and finally to an extended-open state[1, 4, 5]. Concerning the β-integrin subunit, the extended-open conformation is reflected by the swing-out of the hybrid domain in respect to the βA domain [6]. Molecular dynamics (MD) simulations indicate that force supports this hybrid domain swing-out and thereby leads to full integrin activation[4, 7, 8]. These theoretical studies are supported by multiple examples where mechanical forces regulate integrin functions, structural elements of the adhesome, and thus integrin-mediated adhesions[9-15].
The best-studied class of integrins is the group of RGD-binding integrins sharing the ability to interact with an exposed Arg-Gly-Asp peptide in their ligands[16]. Promiscuity between ligands and receptors is especially common for these RGD-integrins. For example, αVβ3 integrin is reported to have the ability to recognize at least 12 different ligands[17]. However, the biological implications of this promiscuity are not well understood.
αVβ3 integrin, initially described as the vitronectin (Vn) receptor[18], is now widely accepted and analyzed in its function as a fibronectin (Fn) receptor[19-23]. However, cancer cells have been reported to upregulate αVβ3 integrin expression[24, 25] paralleled by increased Vn and decreased Fn expression[26, 27]. In endothelial cells, binding of αVβ3 integrin to Vn increases the activation of the VEGF receptor, while this is not the case when αVβ3 integrin is binding to Fn[28].
Thus, analyzing differential effects of Fn and Vn holds the promise to offer improved understanding of integrin signaling and regulation. Most *in vitro* studies on integrin-ECM interactions have been performed on homogeneously coated substrates, whereas *in vivo*, cells are usually exposed to several

ligands organized in a complex 3D environment. We have recently developed a method to produce microstructured, differential Fn/Vn substrates that enable us to analyze the influence of Fn and Vn on a subcellular scale[13, 29]. Here, we combine this method with super-resolution microscopy and super-resolution live cell imaging and reveal a force dependent ligand sensing that permits αVβ3 integrin to discriminate between Fn and Vn. Furthermore, we show that this sensing occurs over a physiological range of tissue stiffness. And finally, we reveal that Vn, together with osteopontin (Opn) and fibrinogen (Fbg), belongs to a class of high-affinity ligands for αVβ3 integrin contrasting with the low-affinity ligand Fn.

Results:

Vitronectin is the preferred ligand for αVβ3 integrin

To study how the simultaneous presentation of two ECM ligands influences binding of αVβ3 integrin, we produced binary Fn/Vn substrates with subcellular structural resolution[29]. 2x2 µm squares of Fn separated by 1 µm gaps were stamped onto a coverslip and the remaining surface was covered with Vn leading to a geometrical coverage of about equal contribution[29]. The quality of substrates was analyzed by fluorescence and atomic force microscopy (Fig. 1a, b). To reveal integrin specific ECM ligand binding, β3-wt integrin GFP was transfected into NIH 3T3 cells expressing low levels of endogenous β3 integrins, and cultured on the patterned surfaces for 2 hrs[29] . Subsequent fixation and immunostaining for paxillin allowed detecting all integrin-mediated cell-matrix adhesions. Imaging with super-resolution structured illumination microscopy (SR-SIM) revealed extended overlap of αVβ3 integrin and anti-paxillin staining (Fig. 1c). However, some paxillin-clusters on Fn were free of αVβ3 integrin, indicating recruitment to endogenous Fn-bound α5β1 integrin (Supplementary Fig. 1b, g). Therefore, these substrates enabled us to analyze the influence of Fn and Vn on αVβ3 integrin adhesion formation at a micrometer scale within single cells. Surprisingly, we found a clear preference of αVβ3 integrin-positive adhesions for Vn with 83.5 % colocalization (Fig. 1d). This preference for Vn was independent of the size of the αVβ3 integrin-mediated adhesion (Fig. 1e), the presence of α5β1 integrin (Supplementary Fig. 1a, f), or the stamping procedure (Supplementary Fig. 1d, j). To study the dynamics of αVβ3 integrin-mediated adhesion formation, we applied SR-SIM live cell imaging. During spreading, cells initiated numerous nascent adhesions (Fig. 1g and Supplementary Video 1 and 2). These adhesions almost exclusively appeared on Vn (Fig. 1f) while some of them were later translocated towards Fn in a centripetal direction to the cell center (Fig. 1g and Supplementary Video 2). In control experiments where Fn was replaced by albumin, αVβ3 integrin-mediated adhesions were constrained to Vn (Supplementary Fig. 1c). This indicates that ligand binding is necessary for localization and stabilization of αVβ3 integrin clusters on Fn-coated squares.
Next, we asked whether the preference for Vn could be explained by different affinities of αVβ3 integrin for these two ligands. Using biolayer interferometry, we analyzed the dissociation constant of purified αVβ3 integrins for Fn and Vn (Fig. 1h, I). Remarkably, Vn only showed dissociation from αVβ3 integrins in the presence of the αVβ3 integrin inhibitor cilengitide (w/o cilengitide: K_d < 1 pM; + 20 µM cilengitide: K_d = 302.6 nM; Supplementary Fig. 2b) similar to previous reports of nondissociable Vn binding[30]. Fn, in contrast, dissociates easily (K_d = 53.98 nM). Thus, the higher affinity of the extracellular head domain of αVβ3 integrin for Vn explains the observed Vn-preference. Accordingly, a chimeric integrin with extracellular β3 and intracellular β1 domains (β3/β1 chimera) showed the same preference for Vn as β3-wt integrin (Supplementary Fig. 1e, h), which emphasized the importance of outside-in signaling in the process of differential ligand recognition. In addition, we performed atomic force microscopy (AFM)-based single-cell force spectroscopy[31, 32] on substrates incorporating adjacent Fn and Vn areas. A living cell attached to the AFM cantilever was alternatingly brought in contact with and retracted from the two ECM components. In respect to different contact times (typically ten force cycles per cell and contact time), the detachment force was determined from force-distance curves collected during cell retraction. Starting after 30 s of adhesion time, a significantly higher force was needed to detach cells from Vn compared to Fn substrates (Fig. 1j).
Together, our experiments revealed that initial αVβ3 integrin-mediated adhesions formed exclusively on Vn, potentially explained by the higher binding affinity of αVβ3 integrin to Vn. However, the question remained why a portion of αVβ3 integrin-mediated adhesions still localized on Fn and how they are stabilized.

Actomyosin contractility regulates the ligand preference of αVβ3 integrin

To test whether mechanical forces are involved in the substrate selection process, we reduced actomyosin contractility with blebbistatin or Y27632. As previously shown[33], both inhibitors increased the number of small, round nascent adhesions in the cell periphery (Fig. 2a, b). In addition, treatment with both inhibitors led to a drastic decrease in colocalization of β3-wt GFP integrin with Fn (Fig. 2g and Supplementary Fig. 1k). Vinculin is well established as an important part of the molecular clutch to

transmit forces from actin to the integrin-ECM bond[13, 34, 35]. Therefore, we analyzed the localization of β3-wt GFP integrin on Fn/Vn substrates for mouse embryonic fibroblasts derived from vinculin knockout mice (MEF Vcl -/-). Indeed, the absence of vinculin led to a decrease in Fn binding of αVβ3 integrin (Fig. 2e, h) that was comparable to the results obtained with the contractility inhibitors (Fig. 2g). Control experiments using wt MEFs (Fig. 2d) and Vcl -/- MEFs re-expressing vinculin mCherry (Fig. 2f) demonstrated that the localization of αVβ3 integrin on Fn can be rescued by vinculin expression. To increase intracellular forces, we overexpressed nonmuscle myosin IIA mApple (NMIIA) in NIH3T3 cells (Fig. 2c). In fact, adding additional NMIIA caused a significant increase of αVβ3 integrin localization on Fn (Fig. 2g). Taken together, these findings indicate that αVβ3 integrin initially binds to Vn and that the subsequent binding of some of these integrins onto Fn requires intracellular forces transmitted via vinculin.

Hybrid-domain swing-out is important for fibronectin binding by αVβ3 integrin

Next, we asked why forces stabilize αVβ3 integrin-mediated adhesions on Fn, while initial αVβ3 integrin adhesions do not form on Fn when exposed to Fn/Vn substrates. It has been shown, that forces enhance integrin activation by influencing the allosteric integrin regulation that leads to the complete hybrid domain swing-out in the headpiece of the β integrin subunit[4, 35, 36]. Therefore, we determined the influence of the allosteric regulation of αVβ3 integrins on their ligand preference by using chemical activation (Fig. 3a) or established integrin mutations (Fig. 3b-d): (i) Mn^{2+} treatment shifts the integrin equilibrium to the extended-closed conformation[37, 38], (ii) the β3-VE mutant increases the affinity for talin 20-fold leading to increased integrin activation[29], (iii) β3-D723A interrupts the inhibitory salt-bridge at the cytoplasmic side of the membrane between the αV- and β3-subunits[39], and (iv) β3-N305T leads to a constitutive hybrid domain swing-out and slower integrin dynamics[40, 41]. On binary choice substrates, only β3-N305T expressing cells showed a significant increase of colocalization between αVβ3 integrins and Fn (Fig. 3j), while Mn^{2+} treatment and the intracellular activating mutations (β3-VE and β3-D723A) caused no significant difference. Next, we tested whether the conformational changes caused by the β3-N305T mutation are accompanied by the ability to initiate adhesions on Fn by using live cell SR-SIM (Fig. 3i and Supplementary Video 3) and compared this to the β3-VE mutation (Supplementary Video 4). In both cases, spreading cells initiated most αVβ3 integrin-mediated adhesions on Vn. In contrast, only cells expressing β3-N305T also formed numerous adhesions on Fn (Fig. 3k). Interestingly, combining β3-wt + Mn^{2+} or the mutations β3-VE and β3-D723A with a blebbistatin treatment led to reduced localization of these integrins on Fn similar to β3-wt + blebbistatin (Supplementary Fig. 1l; unfortunately, β3-N305T could not be combined with blebbistatin treatment). Thus, allosteric activation without hybrid domain swing-out is insufficient to compensate for contractility loss. When combined, the experiments above emphasize the crucial role of a force-mediated hybrid domain swing-out in the binding of αVβ3 integrin to Fn.

Concerning integrins under low force, we made a peculiar observation for all activating mutations and the Mn^{2+} treatment. In the cell center, we observed numerous small adhesions that localize almost exclusively on Vn (Fig. 3 a-d, Supplementary Fig. 3d). These αVβ3 integrin-mediated adhesions recruit talin but not paxillin, vinculin, or actin stress fibers indicating that they are not mechanically coupled and thus are under low intracellular force (Supplementary Fig. 3a-c). Similar integrin clusters have been reported before to appear within minutes after Mn^{2+} addition[39, 41]. The exclusive localization of these low-force αVβ3 integrins on Vn complements our experiments using contractility inhibitors and vinculin -/- cells (Fig. 2g, h).

A correlation of hybrid domain swing-out and Fn binding capacity is further supported by molecular dynamics (MD) simulations. We investigated the binding of the RGD-containing 10th domain of Fn (FnIII10) to extended conformations of αVβ3 integrin exhibiting either the open or closed headpiece. The open headpiece is characterized by hybrid domain swing-out, inward movement of the N-terminal α1-helix, bearing MIDAS and ADMIDAS motifs, and by a piston-like motion of β6-α7 loop and α7-helix[42]. For the MD simulation, a crystal structure of FnIII10-bound to the extended-closed conformation of αVβ3 integrin (PDB: 4MMX) was used as an initial model for FnIII10 binding to αVβ3 integrin. The structure of the extended-open form was prepared by superimposition of βA and hybrid domains from the crystal structure of open αIIbβ3 integrin. After initial short simulations, in order to select replicas based on FnIII10-orientation and interaction energy between the RGD-sequence of FnIII10 and αVβ3 integrin, we proceeded for 100 ns simulations. These MD simulations showed that the orientation of FnIII10 binding to the extended-closed conformation was different to the extended-open (Fig. 3e). Analysis of the interaction energy between the RGD-sequence and αVβ3 integrin showed that FnIII10 is bound more stable to the extended-open conformation (Fig. 3g). Furthermore, RMSF (root mean square fluctuations) of Cα atoms of the RGDSPA-segment showed that this region was more flexible when FnIII10 was bound to the extended-closed integrin (Fig. 3h). In the extended-open conformation, the α1-helix was stable, while in the closed form it was broken (Fig. 3e, f), what caused higher flexibility of the helix (Supplementary Fig. 4a) and potentially of the RGD-motif of bound

FnIII10. The bent conformation of α1-helix is a common feature for a closed integrin headpiece, and the helix unbending upon headpiece opening facilitates the high-affinity RGD binding[43]. Analysis of interactions between ADMIDAS and the β6-α7 loop showed that the loop interacted with the ADMIDAS metal ion only in the extended-closed conformation of αVβ3 integrin (Supplementary Fig. 4b)[7]. These results suggest that FnIII10 - αVβ3 integrin binding is less stable in the extended-closed conformation, and becomes more stable once the integrin is in the extended-open form upon hybrid domain swing-out. Control MD simulations of αVβ3 integrin without FnIII10 confirmed that (i) flexibility of the α1-helix in the extended-closed conformation (Supplementary Fig. 4c), and (ii) changes in the interaction of β6-α7 loop with ADMIDAS metal ion (Supplementary Fig. 4d) are effects of FnIII10 binding. Combined, cell experiments with β3-N305T and MD simulations highlight the necessity of the hybrid domain swing-out for αVβ3 integrin to gain the ability to bind to Fn.

Mechanotransduction is influenced by the integrin/ligand combination

The acting forces on integrins are the combination of intracellular actomyosin contractility and the stiffness-dependent elastic responses of the extracellular matrix. When cells are plated onto substrates with different stiffness, an induction of cell spreading has only been observed on substrates with a Young's modulus E>3-5 kPa[44, 45]. However, a recent report showed that the activating mutation β3-VE led to cell spreading even on soft (E=1.5 kPa) substrates[29], implying that integrin activation determines mechanotransduction. These studies have been performed with cells expressing αVβ3 and α5β1 integrins cultured on Fn. We asked whether force-dependent Fn-binding of αVβ3 integrin may be a critical switch that allows αVβ3-depending spreading on Fn surfaces only on stiffer substrates. Such an effect would be masked in cells expressing α5β1 integrins. Therefore, we employed β1 integrin-deficient GD25 cells and cultured them on elastic substrates with homogeneous Fn coating and compared them to Vn-coated substrates. Cell area and length of paxillin-positive adhesions in cells on both ligands correlated with the stiffness of the elastic gels (Fig. 4 a-f). A quantitative analysis revealed a sigmoidal switch for adhesion length and cell area on substrates with E=5 kPa irrespective of the ligand (Fig. 4g and Supplementary Fig. 5b), suggesting that mechanosensing is regulated independent of integrin ligands. Another explanation could be that preference of αVβ3 integrins for Vn is only valid on glass substrates. Therefore, we combined binary choice substrates with elastic gels (Supplementary Fig. 5a). For cells on soft gels (E≤6.7 kPa), we could not reliably analyze the localization of adhesions on Fn/Vn substrates. However, this was possible on gels with intermediate stiffness, where αVβ3 integrin-mediated adhesions showed the same behavior as on glass (Fig. 4h, i). Paxillin, recruited by αVβ3 integrin in GD25 cells, colocalized with Fn to 15.5 % (E=33 kPa), or 14.3 % (E=219 kPa), respectively, confirming that αVβ3 integrin prefers Vn over a wide stiffness range.

Ligands of αVβ3 integrin belong to two different affinity regimes

Finally, we asked whether our findings for the interaction of αVβ3 integrin with Fn and Vn are also valid for other ligand combinations. We performed additional affinity measurements of αVβ3 integrin and its ligand fibrinogen (Fbg) revealing a high ligand affinity (K_d = 8.15 ± 4.82 nM; Supplementary Fig. 2a) similar to the measurement for Vn (Fig. 1g, h). In addition, we produced binary choice substrates (Fig. 5c) to challenge αVβ3 integrin with Fn and Fbg (Fig. 5a) or with Fn and osteopontin (Opn; Fig. 5b). Interestingly, αVβ3 integrin colocalized with Fbg (Fig. 5d) or Opn (Fig. 5e) to the same amount as with Vn on Fn/Vn substrates (colocalization to Fn: 16.5% on Fn/Vn, 20.2% on Fn/Fbg, 18.3% on Fn/Opn). Next, we tested binary choice substrates composed of Vn/Fbg (Fig. 5 f, j) or Vn/Opn (Fig. 5g, j) and analyzed αVβ3 integrin localization (Fig. 5h, i). On these substrates, αVβ3 integrin was unable to differentiate between both ligands (colocalization to Vn: 45.9% on Vn/Fbg, 50.4% on Vn/Opn). Thus, Vn, Opn, and Fbg may present a class of high-affinity ligands for αVβ3 integrin compared to the low-affinity ligand Fn.

Discussion

Here, we have analyzed the interaction of αVβ3 integrin with two established ligands, Fn and Vn. We show that αVβ3 integrin clearly prefers binding to Vn in biochemical assays as well as in cell culture studies. Most surprising was the inability of αVβ3 integrin to initiate adhesions on Fn in the context of Fn/Vn substrates. Combined with the force-dependent localization of αVβ3 integrin from Vn to Fn, we introduce a hypothesis of force-dependent ligand binding that is supported by several experiments.

The vitronectin receptor

Our findings shed light on the controversy of the binding specificity of αVβ3 integrin towards Vn, and Fn. When αVβ3 integrin was identified, it was coined "the vitronectin receptor" based on its ability to

bind to Vn and, equally important, its inability to bind to Fn[18]. However, later it was shown that αVβ3 integrin also binds to Fn substrates when tested in a cellular context. The data presented here explain these contradicting observations. Indeed, αVβ3 integrin binding under low forces is “the vitronectin receptor” (Fig. 6b) as Pytela and colleagues stated[18]. However, pulling on this integrin increases the ability to bind to Fn (Fig. 6c), thereby explaining the abundant examples of αVβ3 integrin acting as an Fn-receptor in cells and *in vivo*. Recently, publications comparing αVβ3 and α5β1 integrin binding to Fn reported that αVβ3 integrin is more force-sensitive[20] and that single αVβ3 integrins are immobilized to a higher degree than α5β1 integrins[46]. Both reports fit to our data since reducing contractility affected αVβ3 integrin binding on its low-affinity ligand Fn more, than it might affect α5β1 integrin. On the other hand, αVβ3 integrins that are bound to Fn are in a maximally-activated state explaining their spatial immobilization.

Force-regulated conformation

On a structural level, our MD simulations of αVβ3 integrin in the extended-closed conformation emphasized that the hybrid domain swing-out was necessary for Fn binding to αVβ3 integrin. Accordingly, cell experiments with ensembles of αVβ3 integrins only showed increased localization on Fn in the context of the glycan wedge mutant β3-N305T integrin causing extended-open conformation. Due to the lack of structural data on Vn, it was not possible to run MD simulations for αVβ3 integrin and Vn. But several indications let us assume that binding of Vn is already possible for the extended-closed conformation of αVβ3 integrin. First, this scenario would require a very flexible ligand, or ligand sequence exposed on a peptide, to get access to the integrin-binding site even in the bent conformation of αVβ3 integrin. Indeed, many high-affinity ligands for αVβ3 integrin exhibit their RGD-peptide in an extended-loop or non-structured context. In contrast, Fn exhibits its RGD-peptide in a short loop. Thus, steric constraints during ligand binding are more likely in the case of the short RGD loop in Fn. Second, Mn^{2+} treatment activates integrins by shifting the equilibrium to the extended-closed but not to the extended-open conformation[38]. On a cellular level we showed that Mn^{2+} treatment leads to clustered, ligand-bound αVβ3 integrin cluster that exclusively localize on Vn. Additionally, interfering with talin-integrin binding (D723A- and VE-mutation) leads to analogous effects. And third, several MD simulations have shown that pulling on the β-subunit of an integrin favors the extended-open conformation[4, 7, 8]. Accordingly, and suggested by our MD simulations, reducing contractility reduces Fn-binding of αVβ3 integrin, whereas Vn-binding is unaffected.
In total, we offer experimental data for force-regulation of αVβ3 integrin conformation. Importantly, this is linked to an affinity modulation differentiating between high-affinity ligands and Fn (Fig. 6b,c).

Inside-out mechanosensing

The importance of ligand-dependent outside-in signaling let us expect that mechanotransduction via αVβ3 integrin differs for Fn compared to Vn. Surprisingly, we observed a mechanoswitch unaffected by the ligand and comparable to earlier reports using cells expressing different integrins[44, 45]. Thus, mechanosensing seems to be dominated by inside-out signaling. Indeed, Pinon and colleagues[29] have shown that paxillin recruitment by an integrin-talin-interface is necessary for spreading on soft substrates. In contrast, the preference of αVβ3 integrin for Vn over a large range of ECM stiffness indicates that outside-in signaling determines ligand recognition. With regard to this, it is interesting that tissue stiffens during cancer progression[47] and that Vn and αVβ3 integrin are upregulated in many cancer types[24, 27], and in endothelial cells undergoing angiogenesis[48-50]. Stiff tissue leads to enhanced proliferation, due to nuclear YAP localization[45, 51] and increased FAK signaling [52, 53], while Vn leads to proangiogenic effects[28] making this integrin-ligand combination a dangerous risk factor in the development of cancer.

Differential outside-in regulation

Finally, we could show that the ligand-preference of αVβ3 integrin for Vn can be transferred to other ligands, such as Opn and Fbg. Thus, Fn is contrasted by a class of high-affinity ligands. Future studies will show to what extent these ligands differ concerning αVβ3 integrin downstream-signaling and receptor-crosstalk[28]. Such an additional regulatory layer dependent on the integrin-ligand combination increases the possibilities of αVβ3 integrin-mediated outside-in signaling. Accordingly, we assume that analyzing ligand-dependent influences on integrin signaling offers a new avenue for a better understanding of integrins in *in vivo* settings characterized by a complex ECM composition.

Acknowledgements:

This work was supported by the German Research Foundation (Karlsruhe School of Optics and Photonics (KSOP) to M. Bachmann) and by the Baden-Württemberg Stiftung (State Scholarship to M.

Schäfer). We thank Academy of Finland for financial support (grant no. 290506 to V. Hytönen) and acknowledge CSC – IT center for science for computational resources and EDUFI (former CIMO) for postdoctoral fellowship for V. Mykuliak. Swiss National Science Foundation supported the work of B. Wehrle-Haller (31003A_166384).

Figures:

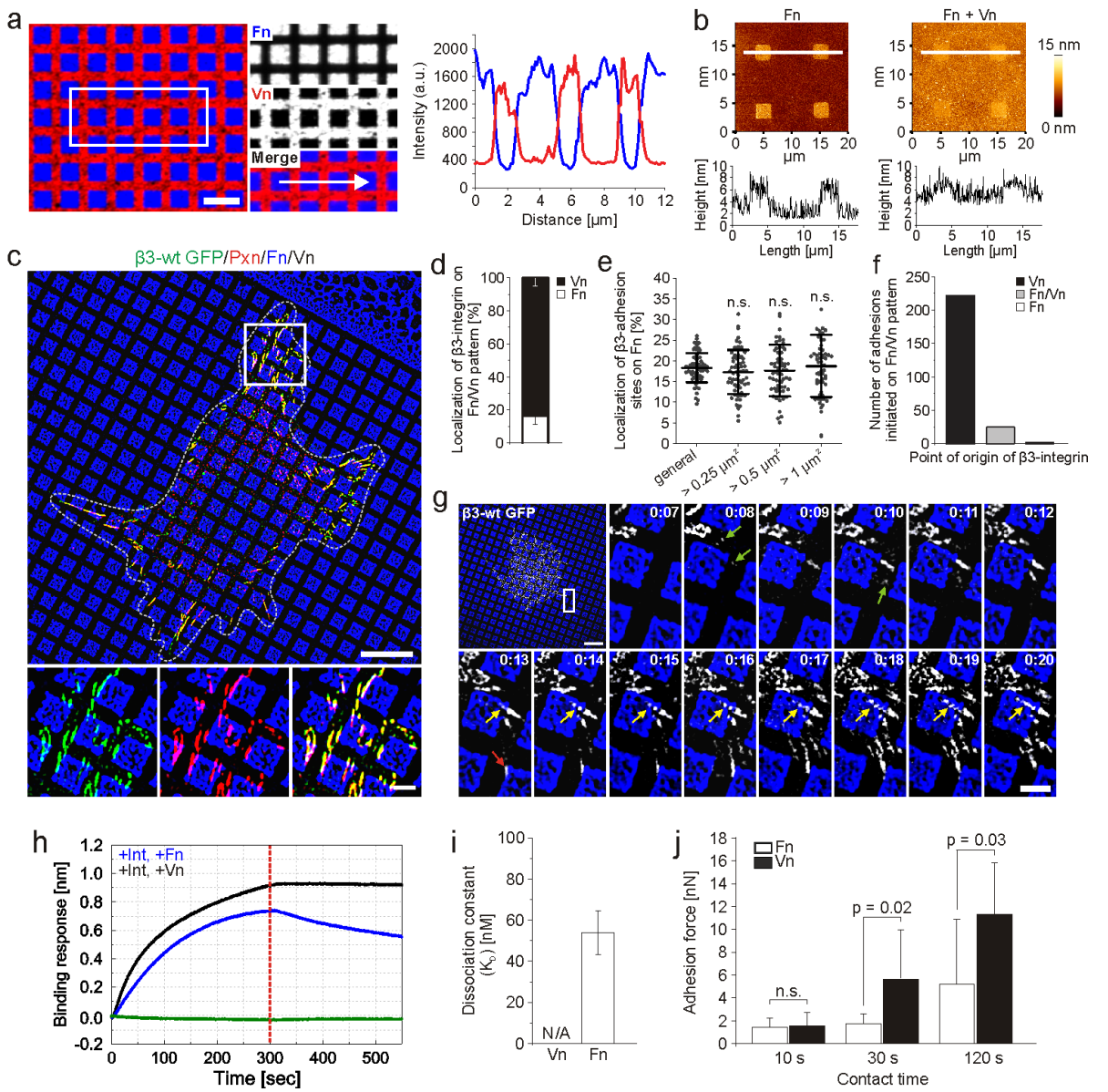

Figure 1: αVβ3 integrin favors binding to vitronectin (Vn) compared to fibronectin (Fn). (**a**) Microcontact printing of 2x2 µm squares of Alexa Fluor 647 labeled Fn (blue) onto glass cover slips and backfilling the pattern with Alexa Fluor 568 labeled Vn (red) leads to differential Fn/Vn patterns as shown by the fluorescence intensity profile along the arrow. Geometrical coverage varies dependent on the pattern quality: 44-49% Fn, 56-51% Vn. (**b**) Height profiles of Fn patterns (left) and Fn/Vn patterns (right) measured with atomic force microscopy (AFM) in contact mode. Profiles along the white lines indicate a monolayer of Fn and a uniform topography of the binary choice substrates. (**c**) Super-resolution structured illumination microscopy (SR-SIM) image of a NIH 3T3 cell transfected for β3-wt GFP integrin (green), cultivated on a Fn/Vn pattern (Fn in blue), and immunostained for paxillin (red). The cell contour is outlined with a dashed white line. (**d**) Quantification of colocalization of β3-wt GFP integrin with Fn or Vn for fixed cells (n = 66; N = 4). (**e**) Quantification of colocalization of β3-wt GFP integrin with Fn for all adhesions ("general") or only for those longer than the indicated threshold (re-analysis of the data from **d**). (**f**) Total number of αVβ3-mediated adhesions that initiated on Vn, Fn, or at the Fn/Vn-interface for cells imaged with live cell SR-SIM. Quantification is based on 246 initiated adhesions from six cells out of three independent experiments. (**g**) NIH 3T3 cell transfected for β3-wt GFP integrin (white) seeded on Fn/Vn patterns (Fn in blue) was monitored with live cell SR-SIM (also see Supplementary Video 1). Magnifications show initiation and maturation of αVβ3-mediated adhesions (time is given in h:min). Green arrows point to newly established adhesions. Yellow arrows follow adhesions that initiated on Vn while they translocate to Fn. The red arrow at 13 min indicates an

adhesion that appeared at the Fn/Vn-interface. (**h**) Representative curves for Fn and Vn association (0 sec to 300 sec) and dissociation (300 sec to 550 sec) to αVβ3 integrin measured with biolayer interferometry. (**i**) K_d values for the interaction of purified αVβ3 integrin to Vn or Fn measured with biolayer interferometry (values calculated from n = 9 measurements in N = 3 independent experiments). (**j**) Single-cell force spectroscopy of GD25wt cells (expressing no β1 integrin). Detachment forces on Fn and Vn measured after the indicated contact time points. Typically 10 force measurement repetitions were performed for each cell and time point, and a total of 8 cells were tested. (**a, c, d**) Scale bars: 10 µm in overviews, 2 µm in zoom-ins.

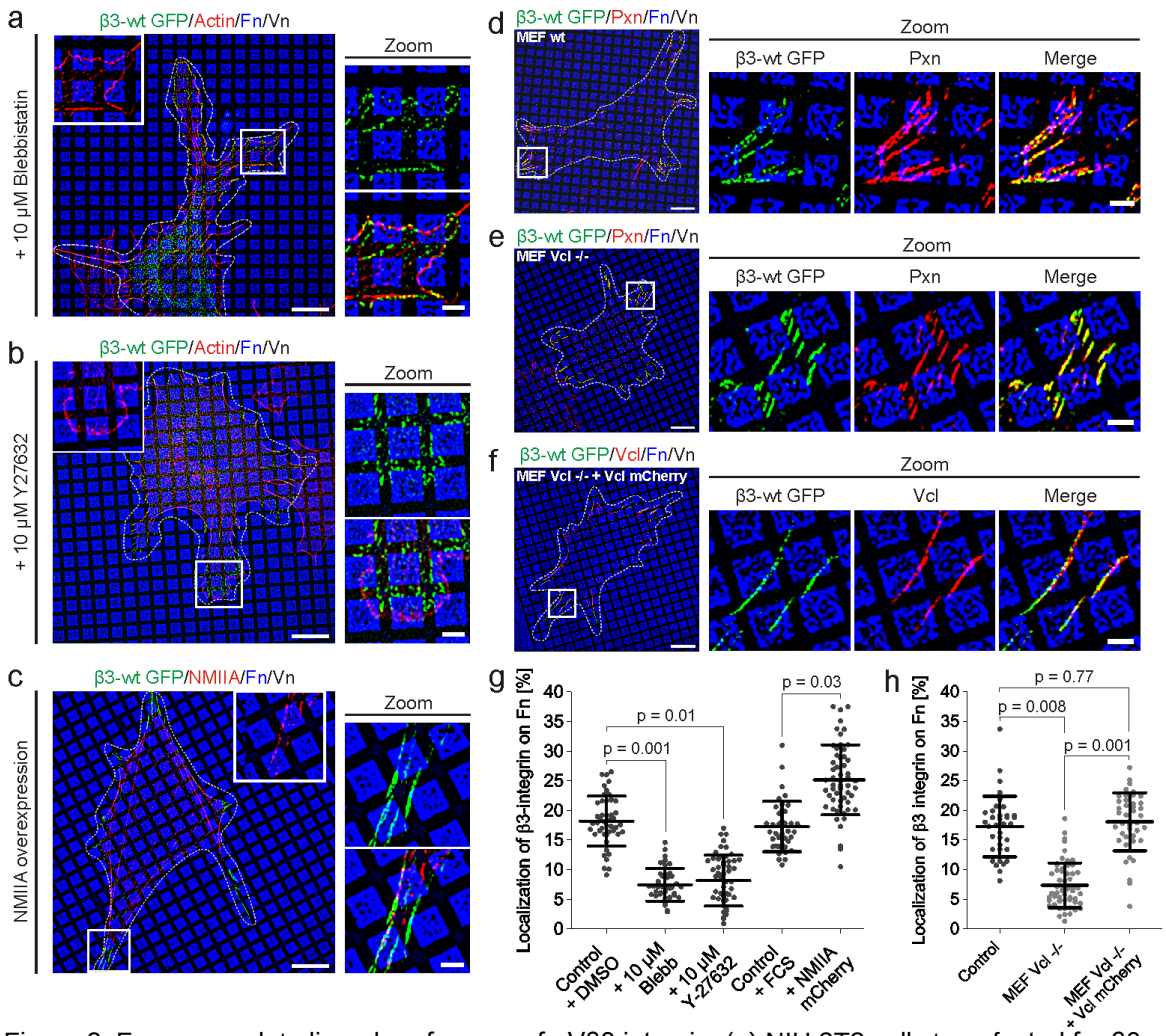

Figure 2: Forces regulate ligand preference of αVβ3 integrin. (**a**) NIH 3T3 cells transfected for β3-wt GFP integrin (green) were cultured on Fn/Vn substrates (Fn in blue) in presence of blebbistatin and after fixation stained for actin (red). (**b**) NIH 3T3 cells treated with Y27632. (**c**) NIH 3T3 cells transfected for β3-wt GFP integrin (green) and myosin IIA mApple (NMIIA; red) with FCS present in the medium. (**d**) MEF wt or (**e**) MEF vinculin knockout cells (MEF Vcl -/-) transfected for β3-wt GFP integrin (in green) and immunostained for paxillin (Pxn; red). (**f**) MEF Vcl -/- cells transfected for β3-wt GFP integrin (green) and Vcl mCherry (red). (**g**) Quantifications of colocalization of β3-wt GFP with Fn for cells treated as described in **a-c** (control + FCS: n = 66, N = 3; control + DMSO: n = 46, N = 3; + 10 µM blebbistatin: n = 40, N = 3; + 10 µM Y-27632: n = 54, N = 3; + NMIIA mCherry: n = 55, N = 3). (**h**) Quantifications of colocalization of β3-wt GFP with Fn for cells treated as described in **d-f** (control: n = 38, N = 3; MEF Vcl -/-: n = 57, N = 3; MEF Vcl -/- + Vcl mCherry: n = 42, N = 3). (**a-f**) All fluorescent images were acquired with SR-SIM. White dashed lines indicate the cell outline. Scale bar: 10 µm in overview images, 2 µm in zoom ins.

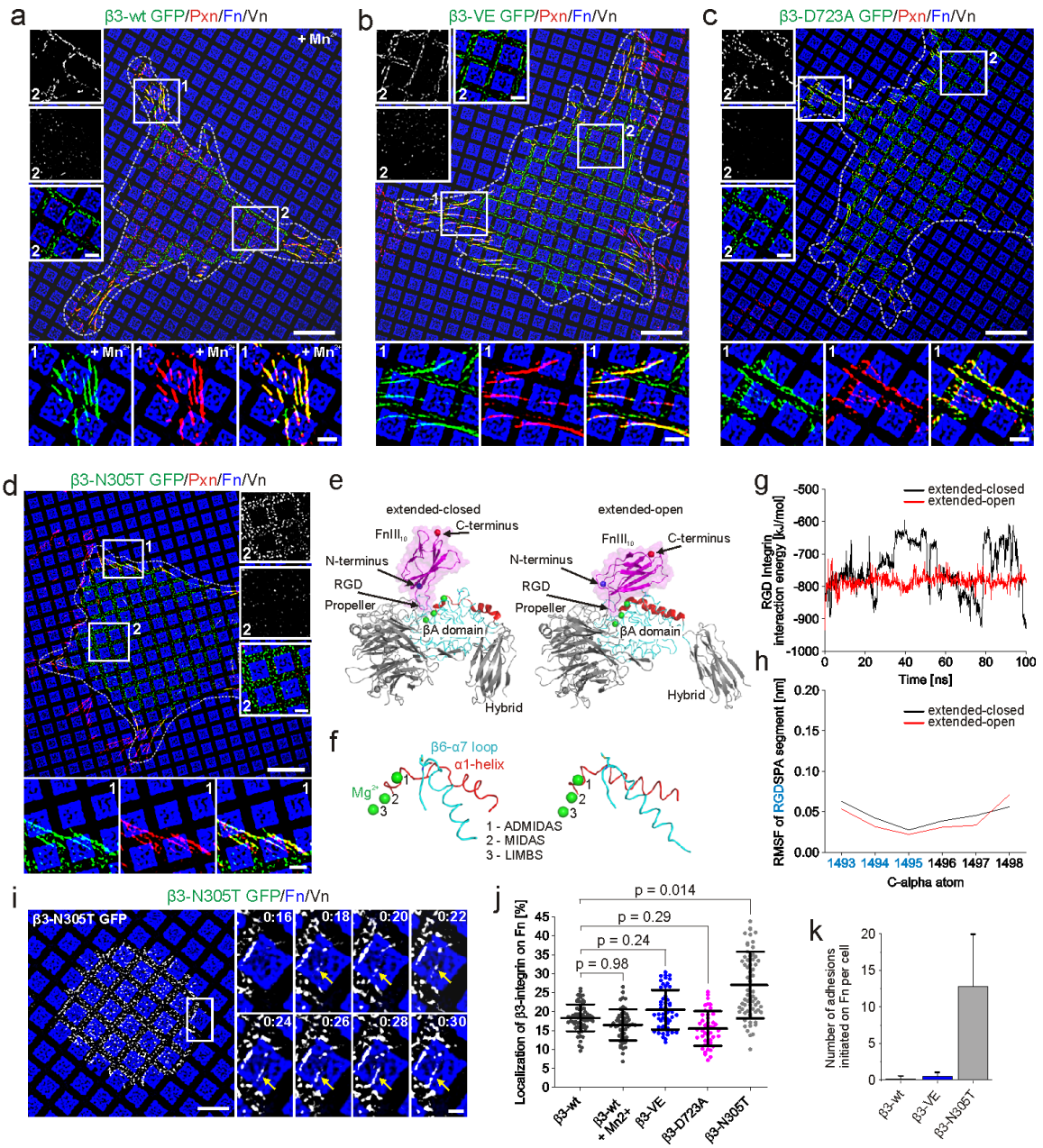

Figure 3: Hybrid domain swing-out is necessary for αVβ3 integrin binding to FN. (**a**) NIH 3T3 cell transfected for β3-wt GFP integrin (green). 1 mM Mn^{2+} was added to the medium 30 min before fixation. (**b**) NIH 3T3 cell transfected for β3-VE GFP integrin (green), or (**c**) for β3-D723A GFP integrin (green), or (**d**) for β3-N305T GFP integrin (green). All cells (**a-d**) were fixed and immunostained for paxillin (Pxn; red). Zoom ins depict adhesions in the cellular periphery (1) or the cell center (2). (**e**) Snapshot of extended-closed and extended-open conformation of FnIII10-bound αVβ3 of a molecular dynamics (MD) simulation. (**f**) The conformation of α1-helix (residues 121 to 145) and β6-α7 loop in extended-closed (left) and extended-open (right) conformation with metal ions at the indicated coordination sites. (**g**) Interaction energy between the RGD motif of FnIII10 and integrin over time of the MD simulation. (**h**) Root mean square fluctuation (RMSF) of the RGDSPA sequence of FnIII10 bound to integrin with blue highlighting the RGD amino acids. (**i**) Live cell SR-SIM imaging of a NIH 3T3 cell transfected for β3-N305T GFP integrin (white) spreading on Fn/Vn substrates (Fn in blue). Yellow arrows indicate an αVβ3 integrin-mediated adhesion that initiated on Fn. (**j**) Quantifications of colocalization of β3-wt GFP with Fn for cells treated as described in **a-d** (β3-wt: replot of the data from Fig. 1d; β3-wt + Mn2+: n = 55, N = 3; β3-VE: n = 54, N = 3; β3-D723A: n = 43, N = 3; β3-N305T: n = 66, N = 4). (**k**) Number of αVβ3 integrin-mediated adhesions per cell that initiated on Fn for NIH 3T3 cells transfected with the indicated integrin (β3-wt is a replot of the data in Fig. 1f; β3-VE: six cells analyzed out of three independent experiments; β3-N305T: six cells analyzed out of four independent experiments). (**a-d, f**) Scale bars: overview images 10 µm, zoom-ins 2 µm. White dashed lines indicate the cell outline. Images acquired with SR-SIM.

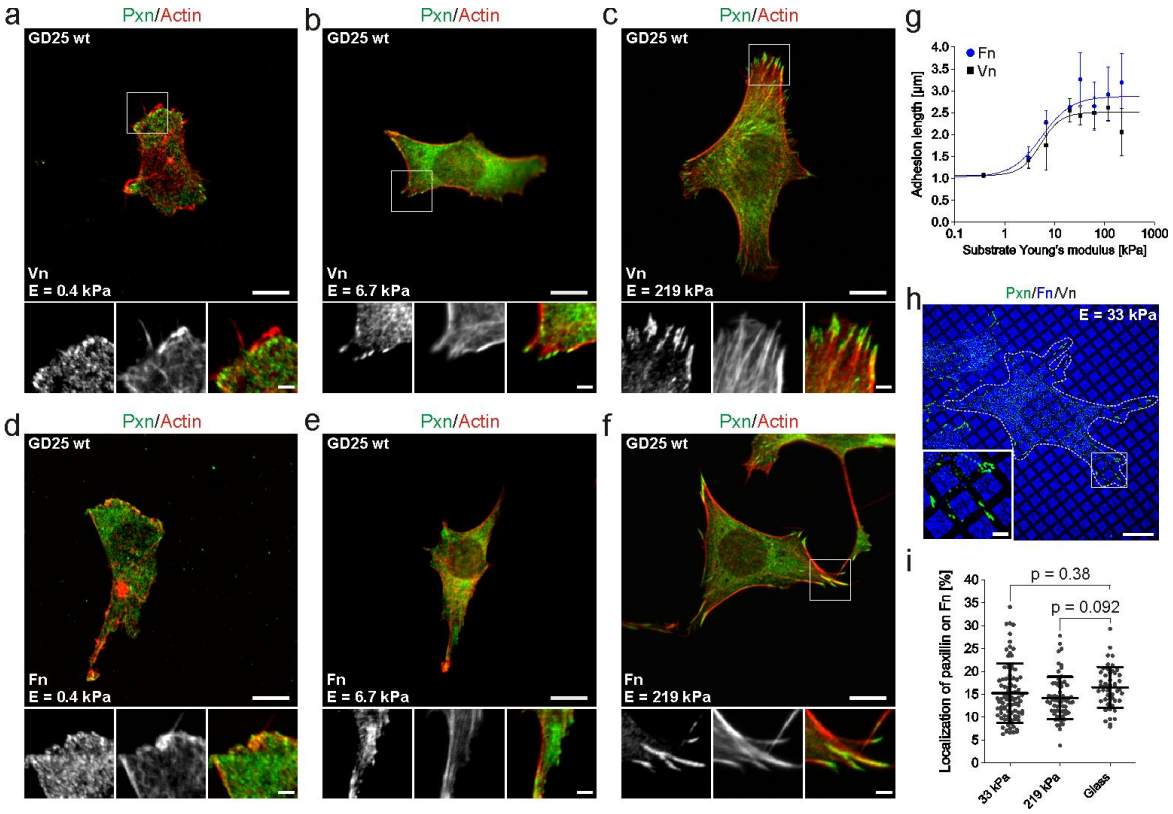

Figure 4: αVβ3 integrin mediates mechanotransduction and prefers Vn over a wide stiffness range. (**a-f**) GD25wt were cultured on elastic polyacrylamide gels of the indicated Young's modulus (E) and stained for paxillin (green) and actin (red). Cells were imaged with diffraction limited microscopy. Gels were coated homogeneously (**a-c**) with Vn or (**d-f**) with Fn. (**g**) Length of paxillin-stained adhesions (longest 25% only) was plotted against the Young's modulus for cells on Vn (black data points) or Fn (blue data points) revealing a mechanical switch for both ligands around 5 kPa (see Supplementary Table 1 for number of analyzed cells; N = 3 for all conditions). (**h**) Immunostained GD25wt cell (paxillin: green; Fn: blue) on a gel with a Young's modulus of E = 33 kPa functionalized with Fn/Vn patterns and imaged with SR-SIM. The zoom in highlights the preferred localization of adhesions on Vn. White dashed line indicates cell outline. (**i**) Quantification of the colocalization of paxillin with Fn for cells grown on Fn/Vn pattern printed on glass (n = 36, N = 3), gels with E = 33 kPa (n = 93, N = 3), or gels with E = 219 kPa (n = 64, N = 3). (**a-f, h**) Scale bar: 10 µm in overviews, 2 µm in zoom-ins.

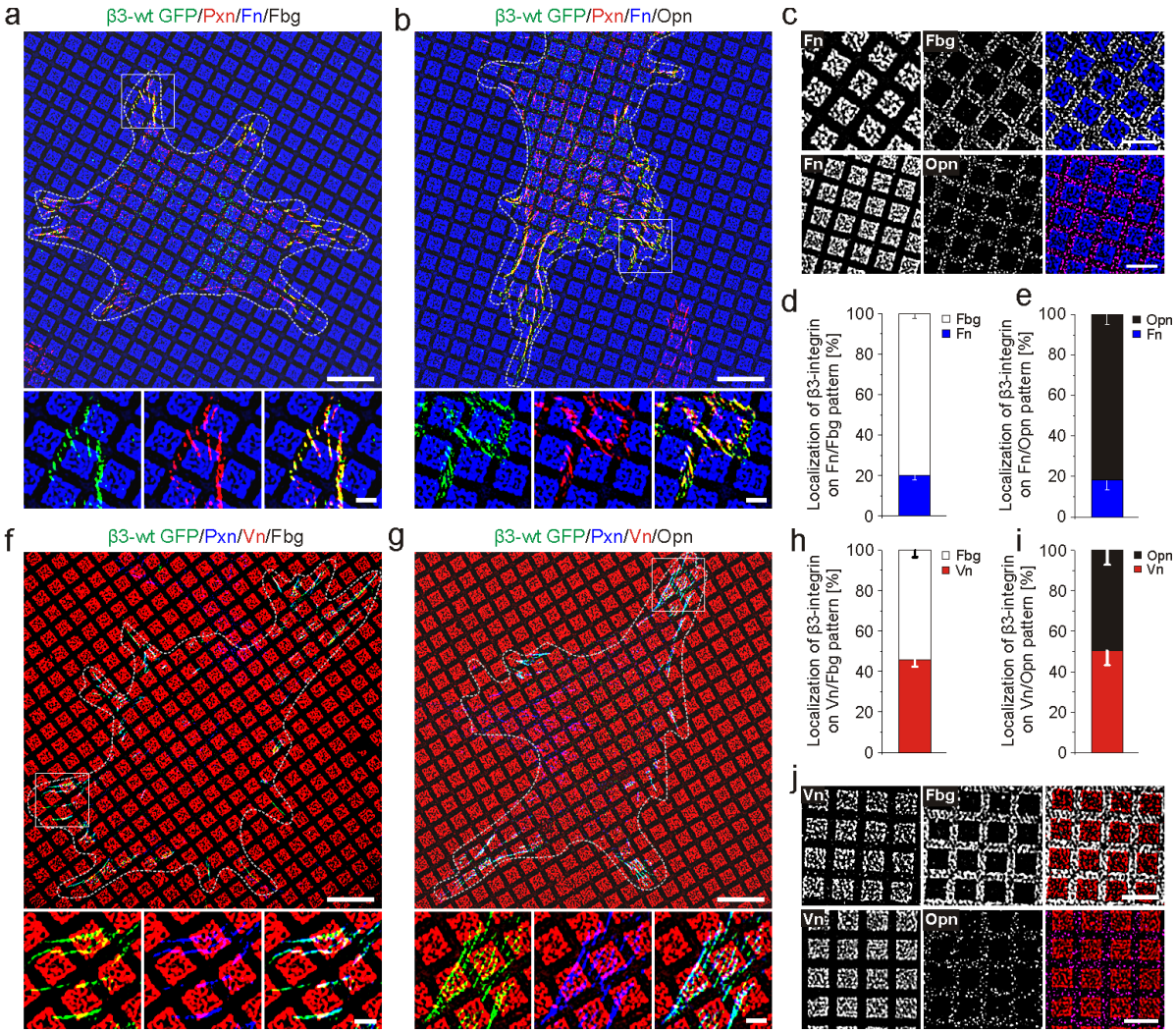

Figure 5: Vitronectin (Vn), osteopontin (Opn), and fibrinogen (Fbg) are high-affinity ligands for αVβ3 integrin. (**a**) Fn squares (blue) were stamped onto cover slips and the remaining area was backfilled with Fbg (black). NIH 3T3 cells transfected for β3-wt GFP integrin (green) cultured on Fn/Fbg substrates in the presence of 1% FCS and immunostained for paxillin (red). (**b**) Cell on a Fn/Opn pattern. (**c**) Staining of Fn/Fbg (Fn in blue; Fbg in white) and Fn/Opn (Fn in blue; Opn in magenta) patterns revealing successful protein separation. (**d**, **e**) Quantification of the colocalization of β3-wt GFP with indicated ECM proteins for cells cultured on Fn/Fbg (n = 69, N = 4) or Fn/Opn substrates (n = 53, N = 3). (**f**) Vn squares (red) were stamped on cover slips and the remaining area was backfilled with Fbg (black). NIH 3T3 cells transfected for β3-wt GFP integrin (green) cultured on Fn/Fbg substrates in presence of 1% FCS and immunostained for paxillin (blue). (**g**) Cell on a Vn/Opn pattern. (**h**, **i**) Quantification of the colocalization of β3-wt GFP with indicated ECM proteins for cells cultured on Vn/Fbg (n = 57, N = 3) or Vn/Opn substrates (n = 45, N = 3). (**j**) Staining of Vn/Fbg (Vn in red; Fbg in white) and Vn/Opn (Vn in red; Opn in magenta) patterns revealing successful protein separation. Scale bars: (**a**, **b**, **f**, **g**) 10 µm in the overview, 2 µm in the zoom in, (**c, j**) 5 µm. (**a**, **b**, **f**, **g**) White dashed lines indicate cell outline. All images acquired with SR-SIM.

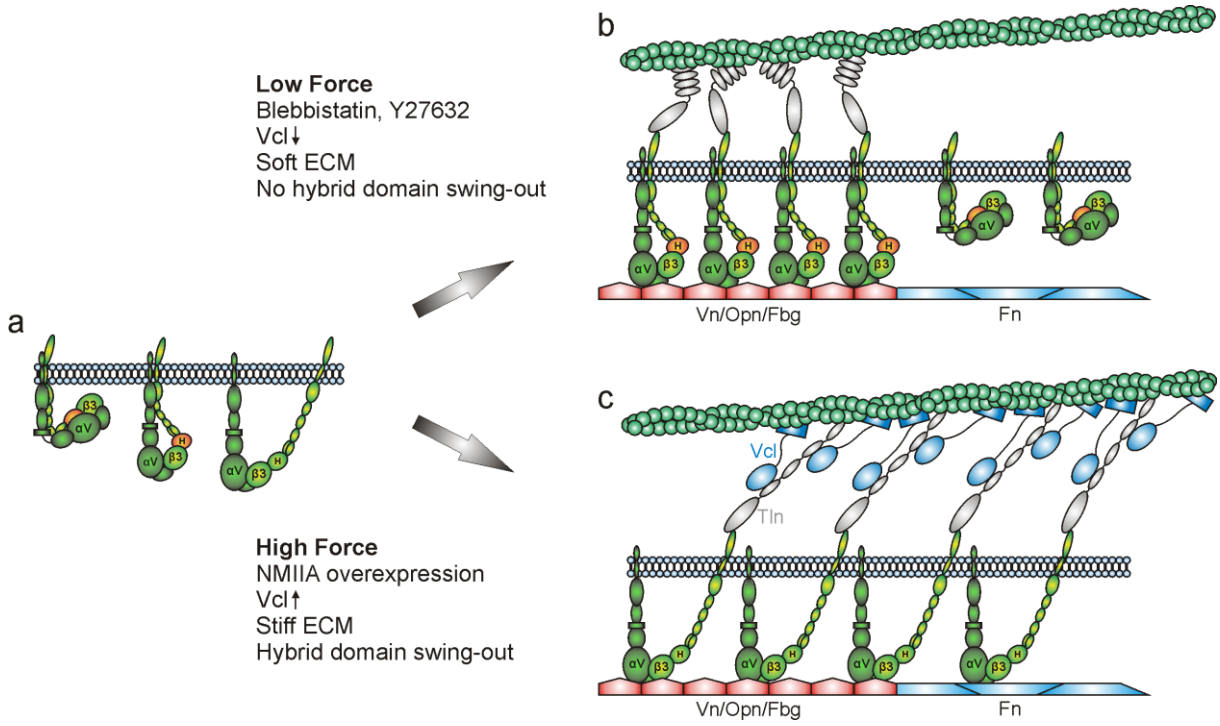

Figure 6: Model for the regulation of αVβ3 integrin by mechanical force and outside-in signaling. (**a**) Conformation of αVβ3 integrin in bent, extended-closed, and extended-open conformation (from left to right). Hybrid domain swing-out in the β3 subunit is coupled to the extended-open conformation indicated by the color change of the hybdrid domain from orange to green. (**b**) αVβ3 integrin in a low-contractile state (either caused by contractility inhibition, by missing vinculin (Vcl; simplified with head and tail region) activation, or by a soft substrate) favors binding to high-affinity ligands like Vn/Opn/Fbg. (**c**) In contrast, a high-contractile state of αVβ3 integrin (either caused by elevated myosin levels (NMIIA overexpression), vinculin binding to stretched talin (Tln; simplified structure with head domain and reduced number of rod domains), or by a stiff substrate), favors the hybrid domain swing-out enabling Fn binding and in consequence a shift of αVβ3 integrin to Fn.

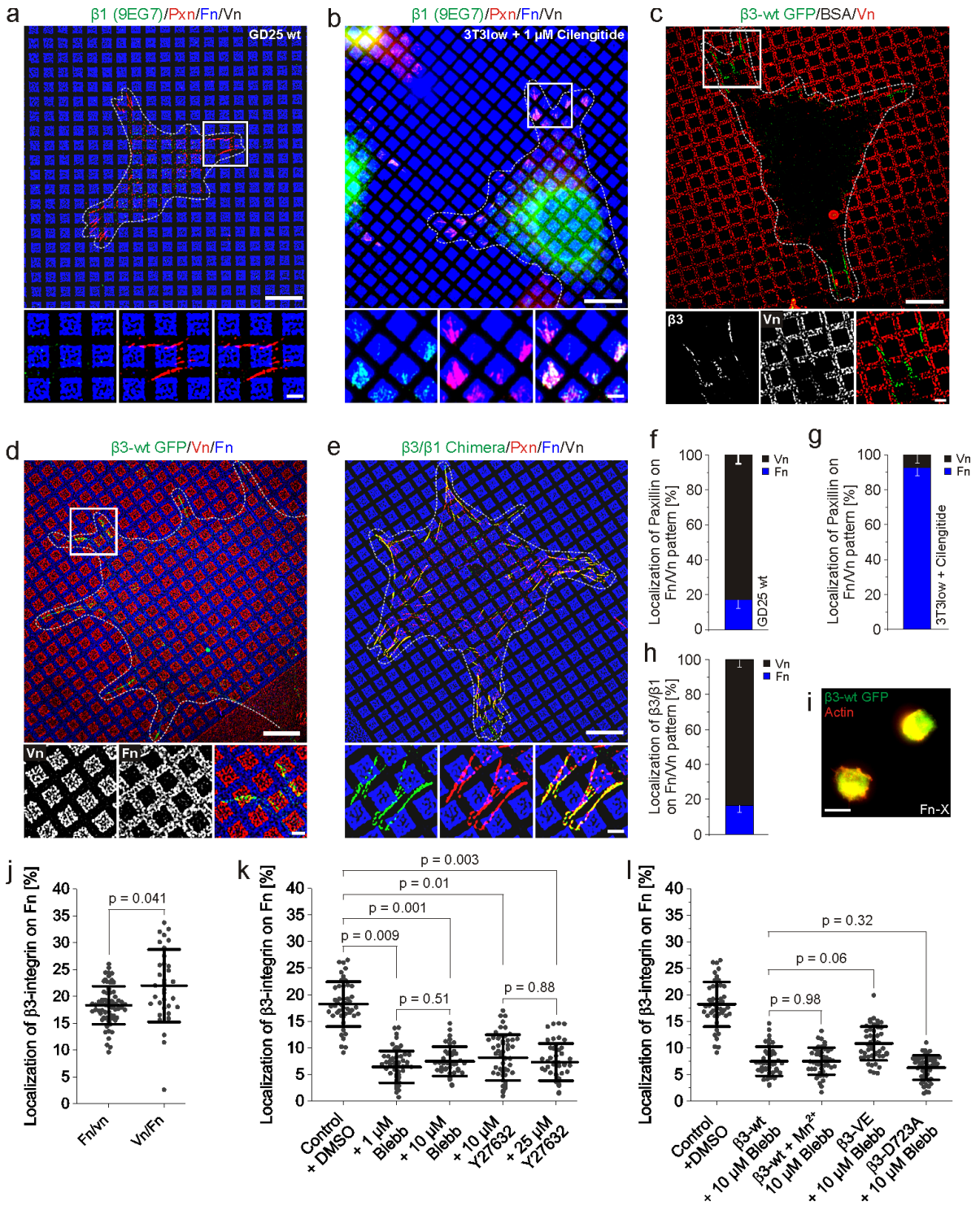

Supplementary Figure 1: (**a**) GD25wt cells cultured on Fn/Vn substrates (Fn in blue) and immunostained for β1 integrin (green) and paxillin (red). GD25wt cells express no β1 integrin (shown by the immunostaining for β1 integrin; left zoom in and merge with paxillin on the right). (**b**) NIH 3T3 cells cultured on Fn/Vn substrates (Fn in blue) and immunostained for β1 integrin (green) and paxillin (Pxn; red). Cilengitide, an αVβ3 integrin inhibitor, was added 30 min before fixation. Paxillin is restricted to Fn. (**c**) Bovine serum albumin (BSA) was stamped and backfilled with Vn (red; labeled by immunostaining). NIH 3T3 cells transfected for β3-wt GFP integrin were cultured on these substrates. Zoom ins show that clustered αVβ3 integrin is not present on BSA. (**d**) Vn labeled with Alexa Fluor 568 (red) was stamped and then overlaid with Alexa Fluor 647 labeled Fn (blue). NIH 3T3 cells were transfected for β3-wt integrin (green) and cultured on these Vn/Fn substrates. (**e**) NIH 3T3 cells were transfected for a β3/β1 integrin chimera (green) with the extracellular part of β3 integrin and the transmembrane and cytoplasmic part of β1 integrin. These cells were cultured on Fn/Vn substrates (Fn in blue) and immunostained for paxillin (red). (**f**) Quantification of paxillin colocalization with Fn in

GD25wt cells treated as described in **a** (n = 36, N = 3). The same data set is used in Fig. 4g. (**g**) Quantification of paxillin colocalization with Fn in NIH3T3 cells treated as described in **b** (n = 27, N = 4). (**h**) Quantification of β3/β1 integrin chimera colocalization with Fn in NIH3T3 cells treated as described in **e** (n = 38, N = 3). (**i**) NIH 3T3 cells transfected for β3-wt GFP integrin cultured on heat-inactivated Fn (Fn-X) that was used together with native Fn during stamping (see Material & Methods). Cells are unable to spread and to cluster integrins on this substrate. (**j**) Quantification of β3 integrin colocalization with Fn in NIH3T3 cells treated as described in **d**. Category "Fn/Vn" is a replot of Fig. 1d (Vn/Fn: n = 38, N = 3). (**k**) Quantification of β3 integrin colocalization with Fn in NIH3T3 cells transfected for β3-wt integrin and cultured on Fn/Vn substrates. Cells cultured in presence of blebbistatin or Y27632 at the indicated concentrations. Values of 10 µM inhibitor concentration and DMSO control are replotted from Fig. 2g (+ 1 µM Blebb: n = 51, N = 3; + 25 µM Y27632: n = 56, N = 3). (**l**) Quantification of β3 integrin colocalization for the indicated mutations with Fn in NIH3T3 cells transfected for β3-wt integrin and cultured on Fn/Vn substrates. 30 min before fixation blebbistatin (and Mn^{2+} where indicated) was added at the indicated concentrations. Values of DMSO control and "β3-wt +10 µM Blebb" are a replot of Fig. 2g (β3-VE+10 µM Blebb: n = 55, N = 3; β3-wt+Mn^{2+} +10 µM Blebb: n = 45, N = 3; β3-D723A+10 µM Blebb: n = 49, N = 3). (**a-e**) White dashed lines in overview images indicate cell outlines. Scale bar: 10 µm in the overview and 2 µm for the zoom in. All fluorescent images except **b** were acquired with SR-SIM.

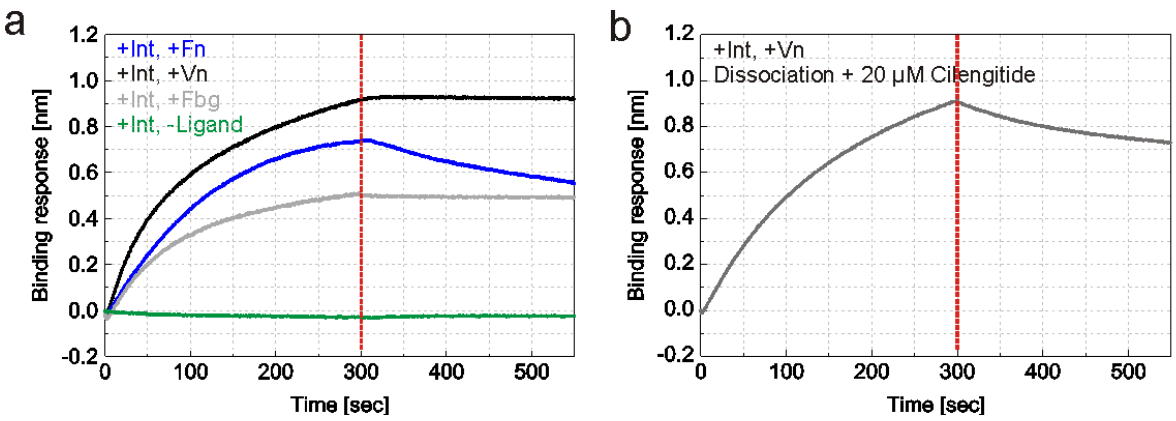

Supplementary Figure 2: (**a**) Association (0 – 300 s) and dissociation (300 – 550 s) curves for the interaction of the indicated ECM proteins with purified αVβ3 integrin. The measurements were performed with biolayer interferometry (representative curves from n = 9, N = 3 measurements for each condition). (**b**) Association and dissociation curve for Vn interaction with purified αVβ3 integrin. Cilengitide was present in the dissociation buffer at 20 µM concentration (representative curve from n = 9, N = 3 measurements).

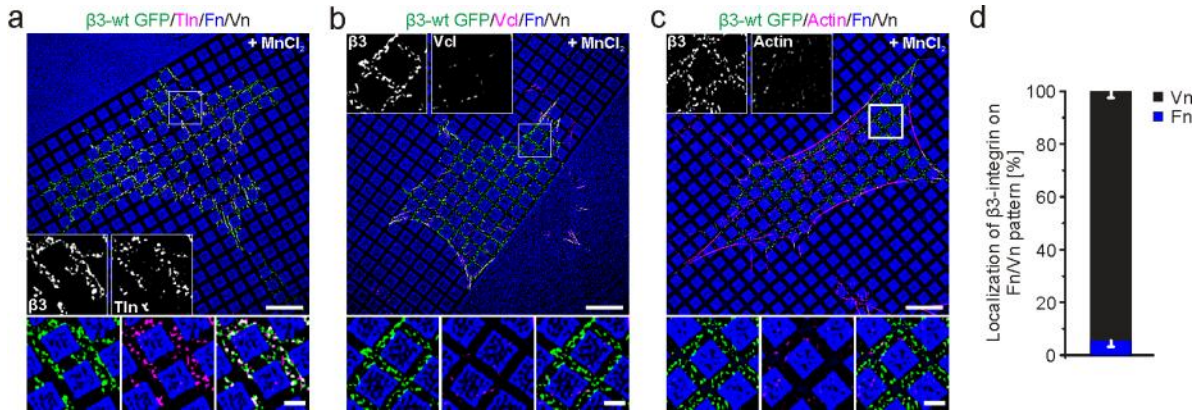

Supplementary Figure 3: (**a-c**) NIH 3T3 cells transfected with β3-wt GFP, cultured on Fn/Vn substrates and treated with 1mM Mn^{2+} 30 min before fixation. Additionally, cells were immunostained for (**a**) talin, (**b**) vinculin, or (**c**) for actin. (**d**) Quantification of β3-wt GFP in central areas of Mn^{2+} treated cells. (**a-c**) Scale bars: 10 µm in the overview, 2 µm in the zoom ins.

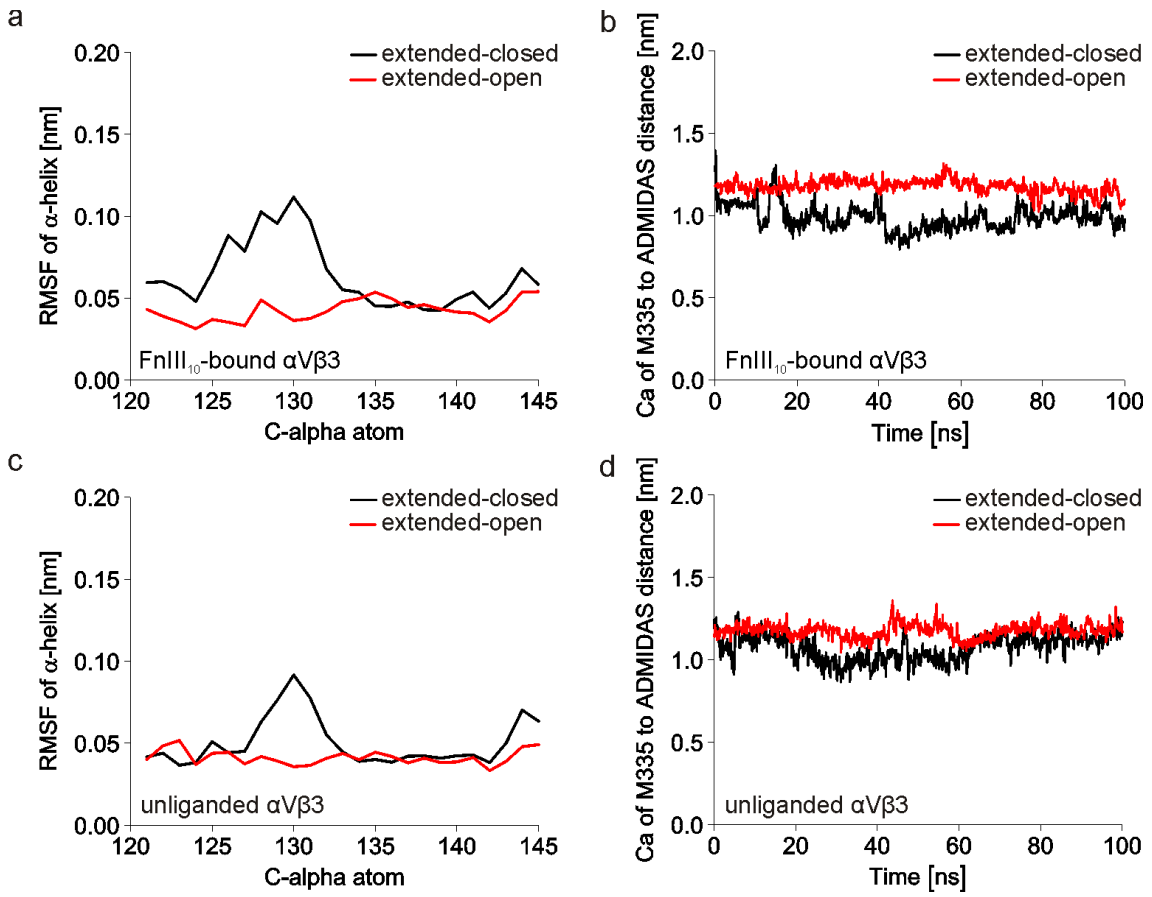

Supplementary Figure 4: (**a, c**) Root mean square fluctuation (RMSF) against indicated C-alpha atoms of α1-helix in (**a**) FnIII10-bound and (**c**) unliganded state of integrin. (**b, d**) The distance between Cα atom of M335 at β6-α7 loop and ADMIDAS ion plotted against the time course of the MD simulation in (**b**) Fn10-bound and (**d**) unliganded state of integrin.

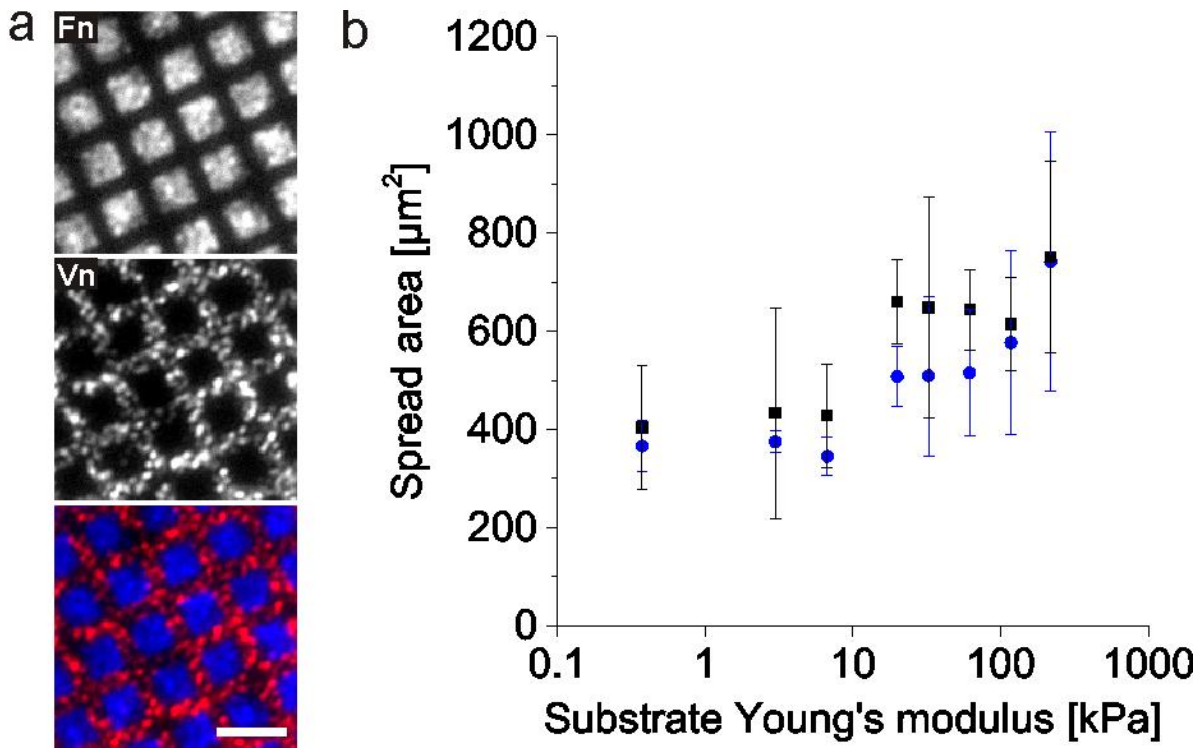

Supplementary Figure 5: (**a**) Protein separation of Fn/Vn patterns tested after transfer of the pattern to polyacrylamide gels by immunostaining for Fn (blue) and Vn (red). (**b**) For cells analyzed in Fig. 4g, cell size was quantified and plotted against the Young's modulus of the gel substrates. Black data points represent Vn coated, blue data points Fn coated elastic gels.

Supplementary Table 1: Polyacrylamide gel rigidities measured with AFM. Number of analyzed cells refers to Fig. 4g and Supplementary Fig. 5b.

Young's module [Pa] **mean ± standard deviation**	**acrylamide, final concentration [%]**	**bisacrylamide, final concentration [%]**	**analyzed cells on Fn**	**analyzed cells on Vn**
0.4 ± 0.08	4	0.03	22	22
3.0 ± 0.98	5.5	0.04	25	33
6.7 ± 1.95	7.46	0.04	25	31
20.1 ± 4.87	7.49	0.10	29	40
32.6 ± 9.38	7.52	0.16	33	39
61.7 ± 27.03	12	0.15	32	37
117.3 ± 20.29	12	0.2	39	42
218.7 ± 44.39	12	0.3	31	33

Methods:

Cell culture, constructs, and transfection

NIH 3T3 cells used in this study are a subclone of NIH3T3 cells that were FACS sorted for low expression of endogenous β3-integrin as described previously[29]. Vinculin-knockout mouse embryonic fibroblasts (MEF Vcl -/-) were kindly provided by Dr. W. H. Ziegler[54]. All cells were grown at 37°C with 5% CO_2 in DMEM (ThermoFischer) supplemented with 10% FCS (Hyclone), and passaged 2-3 times a week, or upon reaching confluency. Transfections were carried out with Lipofectamine 2000 (ThermoFischer) according to manufacturer's instructions. 6 h after transfection, cells were cultured in complete medium for 48h before detachment. cDNA encoding full-length mouse β3-wt GFP integrin expressed in a cytomegalovirus promoter-driven pcDNA3/EGFP vector has been previously described[55]. β3-VE GFP[29], β3-D723A GFP[55], and β3-N305T GFP[55] were derived by substitution from β3-wt GFP integrin construct mentioned before as described in the indicated publications. Vinculin mCherry was a gift from Christoph Ballestrem (Manchester, UK) and mApple-MyosinIIA-C-18 was a gift from Michael Davidson (Addgene plasmid # 54929).

Antibodies and chemicals

Inhibition experiments were performed with blebbistatin (Sigma-Aldrich), with the ROCK inhibitor Y27632 (Sigma-Aldrich), or with the αVβ3 integrin inhibitor cilengitide (Sellekchem) at concentrations as indicated. Cells were fixed for subsequent immunostaining with 4% PFA (Sigma-Aldrich) in PBS. Reagents used for immunostaining were monoclonal mouse antibodies for paxillin (clone 349/Paxillin, BD Biosciences, # 610052), talin (clone 8d4, Sigma-Aldrich, #T3287), vinculin (clone hVIN-1, abcam, #ab11194), vitronectin (clone VIT-2, IgM, Sigma-Aldrich, #V7881) or polyclonal rabbit antibodies for fibronectin (Sigma-Aldrich, #F3648) or osteopontin (GeneTex, #GTX37582). β1-integrin was stained with a monoclonal rat antibody (clone 9EG7, BD Biosciences, # 553715). After primary antibody staining, samples were washed and incubated with antibodies against mouse labeled with Cy3 (Jackson Immunoresearch, #115-165-146), against rabbit labeled with Alexa Fluor 488 (ThermoFischer, #A11070), or with phalloidin coupled to Alexa Fluor 568 (ThermoFischer, #A12380). To visualize anti-Vn staining, secondary antibodies against IgM labeled with Cy3 were used (Dianova, #115-166-075). Primary rat antibodies were visualized with preadsorbed, Alexa Fluor 488 labeled secondary antibodies (ThermoFischer, #A11006) and primary mouse antibodies were in this case visualized with preadsorbed, Cy3 labeled antibodies (Dianova, #111-165-144) to avoid cross-reactivity of secondary antibodies. Direct labeling of Fn, Fbg, and Vn was performed according to manufacturer's protocol with Alexa Fluor 568 (ThermoFischer, # A10238) or Alexa Fluor 647 (ThermoFischer, #A20173).

Microcontact printing

Silicone stamps for microcontact printing of differential substrates were produced as previously described [56] with human plasma fibronectin (Sigma-Aldrich, #F2006 or Millipore, #FC010), human plasma vitronectin (Sigma-Aldrich, #V8379), recombinant human vitronectin (Sigma-Aldrich, #SRP3186), native human fibrinogen (Bio-Rad, #4440-8604), or with osteopontin from bovine milk (Sigma-Aldrich, #O3514). Stamps were incubated for 10 min with a solution of 5 µg/ml Fn and 45 µg/ml heat-inactivated Fn in PBS (see Supplementary Fig. 1i). Alexa Fluor 647 labeled Fn was added to visualize the Fn pattern afterwards. After nitrogen drying, the stamp was pressed onto a glass cover slip for 10 min before it was released. Next, the pattern was covered with Vn at a concentration of 5 µg/ml in PBS for 1 hour at room temperature. Heat-inactivated Fn was produced by heating Fn for 30 min to 90°C and was added to block Vn adsorption in the stamped area. Cells do not spread on heat-inactivated Fn (Supplementary Fig. 1i). For other than Fn/Vn patterns, a total concentration of 50 µg/ml of the stamped protein, and 5 µg/ml of the protein for backfilling was used. All other steps were performed as described. After the final incubation step, patterns were washed with PBS and used directly for cell seeding. Cell detachment was stopped with trypsin inhibitor (Sigma-Aldrich) and cells were seeded in DMEM without FCS if not stated otherwise.

Polyacrylamide gels

Established protocols[29, 57, 58] were adapted to gain polyacrylamide gels of different Young's modulus (stiffness) with homogeneous or with structured ECM. Gels were produced on activated cover slips. Therefore, glass cover slips were cleaned first with propanol and second for 10 min in a plasma cleaner (Technics Plasma GmbH, Germany). This was followed by a silanization (1 h at room temperature, 1 mM 3-(Trimethoxysilyl)propyl methacrylate (Sigma-Aldrich) in toluene). On these cover slips, 60 µl of a mixture of degassed acrylamide, bisacrylamide (Bio-Rad), tetramethylethylenediamine, and ammonium persulfate (TEMED and APS; Sigma-Aldrich) was pipetted with final concentrations of 0.5% APS, 0.1% TEMED, and as mentioned in Supplementary

Table 1. This solution was covered with 10 µl of 1% w/v of Acrylic acid *N*-hydroxysuccinimide ester (NHS acrylate; Sigma-Aldrich) in toluene. Finally, the solution was covered with a cover slip of 18 mm diameter that was either functionalized with a Fn/Vn pattern prepared as described before or that was coated with a 50 µg/ml solution of Fn or Vn for 1h at room temperature. This top cover slip was dried with nitrogen before it was applied to the gel solution. After polymerization, the top cover slip was removed and the gel was covered with PBS. Gel substrates were used directly for cell seeding or were stored overnight at 4°C before cell seeding.
Stiffness of polyacrylamide gels was measured as previously described[45]. Measurements were performed with the atomic force microscope described below. Silicon nitride pyramidal tips with a nominal spring constant of k = 0.01-0.03 Nm^{-1} were used (MLCT, Bruker). An effective half-angle of 20° was used for calculation. For each stiffness 3 gels from 3 independent batches were measured by probing 5 positions in the center of the gel with 5 repetitive measurements. The Hertz model equation for pyramidal tips was fitted to the force-displacement curves.

Microscopy
SR-SIM imaging was performed on a non-serial Zeiss Elyra PS.1 microscope with a 63x oil immersion objective. The grid for SR-SIM was rotated three times and shifted five times leading to 15 frames raw data out of which a final SR-SIM image was calculated with the structured illumination package of ZEN software (Zeiss). Values for calculation were selected for best resolution without causing image artifacts. Channels were aligned by using a correction file that was generated by measuring channel misalignment of fluorescent tetraspecs (ThermoFischer, #T7280). Images of cells on homogeneous polyacrylamide gels were taken using the ApoTome module on a Zeiss AxioimagerZ1 microscope to achieve optical sectioning. For SR-SIM live cell microscopy, incubation chamber was heated to 37°C and cells were imaged every minute. During imaging, cells were cultured in imaging medium (F12 + 25 mM HEPES + 200 mM L-glutamine + 1% penicillin/streptomycin + 10% FCS, pH 7.2). Images were processed as described above.

Atomic Force Microscopy
To prepare adhesion substrates for directly comparative adhesion force spectroscopy, adjacent areas on a Fluorodish 35 (WPI) glass bottom dish were coated with 50 µg/ml BSA (to provide low adhesion for cell capture, see below), 50 µg/ml Fn, or 5 µg/ml Vn solutions and incubated for 1h. Substrates were subsequently rinsed five times with PBS and transferred to CO_2-independent Medium (ThermoFischer). Prior to SCFS experiments, GD25wt cells were transferred to CO_2-independent Medium for 1 h and then trypsinized. Trypsin was subsequently inactivated by adding soybean trypsin inhibitor (Sigma-Aldrich). After centrifugation, the supernatant was removed, and cells were again resuspended in CO_2-independent Medium. SCFS experiments were performed using a CellHesion 200 atomic force microscope (JPK) featuring an extended vertical range of 100 µm. All measurements were performed at 37ºC using a temperature-controlled sample chamber (BioCell from JPK) and tipless 205 µm long V-shaped cantilevers with a nominal spring constant of 0.06 N/m (NP-O from Veeco). To facilitate cell capture, plasma-cleaned cantilevers were functionalized with concanavalin A. After calibrating the sensitivity of the optical lever system and determining the spring constant, cells were pipetted into the sample chamber. A single cell was captured above the BSA coated area by pressing the functionalized cantilever onto the cell with a contact force of 500 pN for 3 s and elevating the cantilever subsequently. To measure cell detachment forces, the cantilever was lowered at a constant speed of 5 µm/s until the cell made contact with the substrate and a preset force of 1.5 nN was reached. Afterwards, the cantilever was held at a constant height for the preset contact time until the cantilever was elevated 80 µm above the substrate surface. Each cell was tested alternatingly on Fn and Vn surfaces (typically 10 force cycle repetitions for each contact time) to determine the differential adhesion strength to both ligands. In total, 8 different cells were tested. Detachment forces were analyzed using the JPK image processing software. From the collected force-distance curves, the maximum detachment forces (maximum cantilever deflection) were determined and plotted as mean ± SD using OriginPro 8.1G. Statistical significance of experiments was tested with a Wilcoxon-based Mann-Whitney U-test using InStat.

Image Analysis
Colocalization, cell area, and adhesion length were analyzed with Fiji software package[59]. A threshold was applied to the intensity of the corresponding fluorescent channel and the area or the length of individual integrin-mediated adhesions was measured with plugins included in Fiji. Colocalization to Fn was quantified by measuring Mander's coefficient of thresholded images by using the Fiji plugin JACoP[60]. Place of adhesion initiation on Fn/Vn substrates was defined by analyzing SR-SIM live cell movies. The fluorescent channel of the integrin staining was analyzed while the Fn channel was hidden. Integrin clusters visible for at least two subsequent time frames were marked with an ellipse in

the ZEN imaging software throughout the movie. Afterwards, the Fn channel was uncovered, and positions of ellipses were counted with respect to FN squares or Vn surrounding the squares. If an integrin cluster initiated at the border of a square with contact to Fn and Vn, it was counted for category Fn/Vn.

Biolayer interferometry measurement

Dissociation constants of αVβ3 integrin binding to different ECM proteins were measured using the BLItz biolayer interferometer (Pall ForteBio). All steps during real-time measurements were performed at room temperature in same buffer conditions (20 mM Tris, 150 mM NaCl, pH 7.4, 1mM $MgCl_2$, 1 mM $CaCl_2$, 0.02% Tween20, 0.1% BSA). Pre-hydrated (10 minutes in integrin buffer) Ni-NTA biosensors (Pall ForteBio) were loaded with 50 µg/ml His-tagged human recombinant αVβ3 integrin (RnD Systems, #3050-AV) following an association phase with 150 µg/ml ECM protein and a dissociation phase (baseline – 45s; loading – 180s; baseline – 45s; association – 300s, dissociation – 300s). Binding curves were corrected for a reference sample, and K_D values were calculated from association rate constants, and dissociation rate constants derived by software from local curve fits corrected for start of association and dissociation. In control experiments, 20 µM cilengitide was added to the integrin buffer during dissociation phase (Supplementary Fig. 2b). A 10 s adjustment step was included.

Molecular Dynamic Simulation

In simulations, we used the structure of FnIII10–bound integrin in extended-closed and extended-open form including propeller, βA, and hybrid domains. Crystal structure of αVβ3 integrin from RCSB Protein Data Bank (ID: 4MMX) was used as a model for the extended-closed integrin. Structure of the extended-open form was prepared by superimposition of βA and hybrid domains from the crystal structure of open αIIbβ3 integrin (ID: 3FCU). Systems containing unliganded αVβ3 were prepared by removing FnIII10 from initial structure. MD simulations were performed using Gromacs ver 2016.1 [61] at the Sisu supercomputer, CSC, Finland. The CHARMM27 force field [62] and explicit TIP3P water model [63] in 0.15 M KCL neutral solution were used. Energy minimization of the system was performed in 25 000 steps using steepest descent algorithm. The system was equilibrated in three phases using harmonic position restraints on all heavy atoms of protein. The first phase of equilibration was performed with NVT ensemble for 100 ps using the Berendsen weak coupling algorithm [64] to control the temperature of the system at 100 K. Integration time step of 2 fs was used in all the simulations. Following NVT, the system is linearly heated from 100 to 310 K over 1 ns using an NPT ensemble at 1 atm of pressure. During this process, the Berendsen algorithm was used to control both temperature and pressure. For the final phase of equilibration and for all subsequent simulations, an NPT ensemble was maintained at 310 K, using V-rescale algorithm [65], and 1 atm as implemented in Gromacs 2016.1. Temperature coupling was applied separately for protein and solution parts. Preparation of structures and analysis was performed using PyMOL 1.7. Interaction energy, which was calculated to evaluate FNIII10 RGD–integrin interactions, is a sum of Lennard-Jones and Coulomb energies.

Statistics

If not stated otherwise, reported values in bar charts are calculated as mean and error bars are representing standard deviation of the mean. In box plots, upper and lower bar indicate standard deviation and the middle bar indicates the mean. Statistical comparisons are calculated with two-tailor Student's t-test if not stated otherwise. All experiments were reproducible and were carried out as independent experiments as often as indicated in the figure legends.

References:

1. Campbell, I.D. & Humphries, M.J. Integrin structure, activation, and interactions. *Cold Spring Harb Perspect Biol* **3** (2011).
2. Hytönen, V.P. & Wehrle-Haller, B. Protein conformation as a regulator of cell-matrix adhesion. *Phys Chem Chem Phys* **16**, 6342-6357 (2014).
3. Zaidel-Bar, R., Itzkovitz, S., Ma'ayan, A., Iyengar, R. & Geiger, B. Functional atlas of the integrin adhesome. *Nat Cell Biol* **9**, 858-867 (2007).
4. Zhu, J. *et al.* Structure of a complete integrin ectodomain in a physiologic resting state and activation and deactivation by applied forces. *Mol Cell* **32**, 849-861 (2008).
5. Su, Y. *et al.* Relating conformation to function in integrin alpha5beta1. *Proc Natl Acad Sci U S A* **113**, E3872-3881 (2016).
6. Zhu, J. & Springer, T.A. Complete integrin headpiece opening in eight steps. *J Cell Biol* **201**, 1053-1068 (2013).
7. Puklin-Faucher, E., Gao, M., Schulten, K. & Vogel, V. How the headpiece hinge angle is opened: New insights into the dynamics of integrin activation. *J Cell Biol* **175**, 349-360 (2006).
8. Dong, X. *et al.* Force interacts with macromolecular structure in activation of TGF-beta. *Nature* **542**, 55-59 (2017).
9. Balaban, N.Q. *et al.* Force and focal adhesion assembly: a close relationship studied using elastic micropatterned substrates. *Nat Cell Biol* **3**, 466-472 (2001).
10. Stricker, J., Aratyn-Schaus, Y., Oakes, P.W. & Gardel, M.L. Spatiotemporal constraints on the force-dependent growth of focal adhesions. *Biophys J* **100**, 2883-2893 (2011).
11. Hytonen, V.P. & Wehrle-Haller, B. Mechanosensing in cell-matrix adhesions - Converting tension into chemical signals. *Exp Cell Res* **343**, 35-41 (2016).
12. Nordenfelt, P., Elliott, H.L. & Springer, T.A. Coordinated integrin activation by actin-dependent force during T-cell migration. *Nature Communications* **7** (2016).
13. Rahikainen, R. *et al.* Mechanical stability of talin rod controls cell migration and substrate sensing. *Sci Rep* **7**, 3571 (2017).
14. Kuo, J.C., Han, X., Hsiao, C.T., Yates, J.R., 3rd & Waterman, C.M. Analysis of the myosin-II-responsive focal adhesion proteome reveals a role for beta-Pix in negative regulation of focal adhesion maturation. *Nat Cell Biol* **13**, 383-393 (2011).
15. Schiller, H.B., Friedel, C.C., Boulegue, C. & Fässler, R. Quantitative proteomics of the integrin adhesome show a myosin II-dependent recruitment of LIM domain proteins. *EMBO Rep* **12**, 259-266 (2011).
16. Hynes, R.O. Integrins: bidirectional, allosteric signaling machines. *Cell* **110**, 673-687 (2002).
17. Humphries, J.D., Byron, A. & Humphries, M.J. Integrin ligands at a glance. *J Cell Sci* **119**, 3901-3903 (2006).
18. Pytela, R., Pierschbacher, M.D. & Ruoslahti, E. A 125/115-kDa cell surface receptor specific for vitronectin interacts with the arginine-glycine-aspartic acid adhesion sequence derived from fibronectin. *Proc Natl Acad Sci U S A* **82**, 5766-5770 (1985).
19. Roca-Cusachs, P., Gauthier, N.C., Del Rio, A. & Sheetz, M.P. Clustering of alpha(5)beta(1) integrins determines adhesion strength whereas alpha(v)beta(3) and talin enable mechanotransduction. *Proc Natl Acad Sci U S A* **106**, 16245-16250 (2009).
20. Schiller, H.B. *et al.* β1- and αv-class integrins cooperate to regulate myosin II during rigidity sensing of fibronectin-based microenvironments. *Nat Cell Biol* **15**, 625-636 (2013).

21. Cao, L. *et al.* Detection of an Integrin-Binding Mechanoswitch within Fibronectin during Tissue Formation and Fibrosis. *ACS Nano* **11**, 7110-7117 (2017).
22. Danen, E.H., Sonneveld, P., Brakebusch, C., Fassler, R. & Sonnenberg, A. The fibronectin-binding integrins alpha5beta1 and alphavbeta3 differentially modulate RhoA-GTP loading, organization of cell matrix adhesions, and fibronectin fibrillogenesis. *J Cell Biol* **159**, 1071-1086 (2002).
23. Balcioglu, H.E., van Hoorn, H., Donato, D.M., Schmidt, T. & Danen, E.H. The integrin expression profile modulates orientation and dynamics of force transmission at cell-matrix adhesions. *J Cell Sci* **128**, 1316-1326 (2015).
24. Preissner, K.T. & Reuning, U. Vitronectin in vascular context: facets of a multitalented matricellular protein. *Semin Thromb Hemost* **37**, 408-424 (2011).
25. Weis, S.M. & Cheresh, D.A. αv Integrins in Angiogenesis and Cancer, in *Cold Spring Harb Perspect Med*, Vol. 1 (2011).
26. Gladson, C.L. The extracellular matrix of gliomas: modulation of cell function. *J Neuropathol Exp Neurol* **58**, 1029-1040 (1999).
27. Gladson, C.L., Wilcox, J.N., Sanders, L., Gillespie, G.Y. & Cheresh, D.A. Cerebral microenvironment influences expression of the vitronectin gene in astrocytic tumors. *J Cell Sci* **108 (Pt 3)**, 947-956 (1995).
28. Soldi, R. *et al.* Role of alphavbeta3 integrin in the activation of vascular endothelial growth factor receptor-2. *EMBO J* **18**, 882-892 (1999).
29. Pinon, P. *et al.* Talin-bound NPLY motif recruits integrin-signaling adapters to regulate cell spreading and mechanosensing. *J Cell Biol* **205**, 265-281 (2014).
30. Orlando, R.A. & Cheresh, D.A. Arginine-glycine-aspartic acid binding leading to molecular stabilization between integrin alpha v beta 3 and its ligand. *J Biol Chem* **266**, 19543-19550 (1991).
31. Langhe, R.P. *et al.* Cadherin-11 localizes to focal adhesions and promotes cell-substrate adhesion. *Nat Commun* **7**, 10909 (2016).
32. Dao, L. *et al.* Revealing non-genetic adhesive variations in clonal populations by comparative single-cell force spectroscopy. *Exp Cell Res* **318**, 2155-2167 (2012).
33. Choi, C.K. *et al.* Actin and alpha-actinin orchestrate the assembly and maturation of nascent adhesions in a myosin II motor-independent manner. *Nat Cell Biol* **10**, 1039-1050 (2008).
34. Thievessen, I. *et al.* Vinculin-actin interaction couples actin retrograde flow to focal adhesions, but is dispensable for focal adhesion growth. *J Cell Biol* **202**, 163-177 (2013).
35. Humphries, J.D. *et al.* Vinculin controls focal adhesion formation by direct interactions with talin and actin. *J Cell Biol* **179**, 1043-1057 (2007).
36. Ciobanasu, C., Faivre, B. & Le Clainche, C. Actomyosin-dependent formation of the mechanosensitive talin-vinculin complex reinforces actin anchoring. *Nat Commun* **5**, 3095 (2014).
37. Li, J. *et al.* Conformational equilibria and intrinsic affinities define integrin activation. *Embo j* **36**, 629-645 (2017).
38. Eng, E.T., Smagghe, B.J., Walz, T. & Springer, T.A. Intact alphaIIbbeta3 integrin is extended after activation as measured by solution X-ray scattering and electron microscopy. *J Biol Chem* **286**, 35218-35226 (2011).
39. Saltel, F. *et al.* New PI(4,5)P2- and membrane proximal integrin-binding motifs in the talin head control beta3-integrin clustering. *J Cell Biol* **187**, 715-731 (2009).

40. Luo, B.H., Springer, T.A. & Takagi, J. Stabilizing the open conformation of the integrin headpiece with a glycan wedge increases affinity for ligand. *Proc Natl Acad Sci U S A* **100**, 2403-2408 (2003).
41. Cluzel, C. *et al.* The mechanisms and dynamics of (alpha)v(beta)3 integrin clustering in living cells. *J Cell Biol* **171**, 383-392 (2005).
42. Arnaout, M.A., Goodman, S.L. & Xiong, J.P. Structure and mechanics of integrin-based cell adhesion. *Curr Opin Cell Biol* **19**, 495-507 (2007).
43. Zhang, C. *et al.* Modulation of integrin activation and signaling by alpha1/alpha1'-helix unbending at the junction. *J Cell Sci* **126**, 5735-5747 (2013).
44. Yeung, T. *et al.* Effects of substrate stiffness on cell morphology, cytoskeletal structure, and adhesion. *Cell Motil Cytoskeleton* **60**, 24-34 (2005).
45. Elosegui-Artola, A. *et al.* Mechanical regulation of a molecular clutch defines force transmission and transduction in response to matrix rigidity. *Nat Cell Biol* **18**, 540-548 (2016).
46. Rossier, O. *et al.* Integrins β1 and β3 exhibit distinct dynamic nanoscale organizations inside focal adhesions. *Nat Cell Biol* **14**, 1057-1067 (2012).
47. Lu, P., Weaver, V.M. & Werb, Z. The extracellular matrix: a dynamic niche in cancer progression. *J Cell Biol* **196**, 395-406 (2012).
48. Leu, S.J., Lam, S.C. & Lau, L.F. Pro-angiogenic activities of CYR61 (CCN1) mediated through integrins alphavbeta3 and alpha6beta1 in human umbilical vein endothelial cells. *J Biol Chem* **277**, 46248-46255 (2002).
49. Drake, C.J., Cheresh, D.A. & Little, C.D. An antagonist of integrin alpha v beta 3 prevents maturation of blood vessels during embryonic neovascularization. *J Cell Sci* **108 (Pt 7)**, 2655-2661 (1995).
50. Brooks, P.C., Clark, R.A. & Cheresh, D.A. Requirement of vascular integrin alpha v beta 3 for angiogenesis. *Science* **264**, 569-571 (1994).
51. Dupont, S. *et al.* Role of YAP/TAZ in mechanotransduction. *Nature* **474**, 179-183 (2011).
52. Bae, Y.H. *et al.* A FAK-Cas-Rac-lamellipodin signaling module transduces extracellular matrix stiffness into mechanosensitive cell cycling. *Sci Signal* **7**, ra57 (2014).
53. Sulzmaier, F.J., Jean, C. & Schlaepfer, D.D. FAK in cancer: mechanistic findings and clinical applications. *Nat Rev Cancer* **14**, 598-610 (2014).
54. Mierke, C.T. *et al.* Vinculin facilitates cell invasion into three-dimensional collagen matrices. *J Biol Chem* **285**, 13121-13130 (2010).
55. Ballestrem, C., Hinz, B., Imhof, B.A. & Wehrle-Haller, B. Marching at the front and dragging behind: differential alphaVbeta3-integrin turnover regulates focal adhesion behavior. *J Cell Biol* **155**, 1319-1332 (2001).
56. Lehnert, D. *et al.* Cell behaviour on micropatterned substrata: limits of extracellular matrix geometry for spreading and adhesion. *J Cell Sci* **117**, 41-52 (2004).
57. Kandow, C.E., Georges, P.C., Janmey, P.A. & Beningo, K.A. Polyacrylamide hydrogels for cell mechanics: steps toward optimization and alternative uses. *Methods Cell Biol* **83**, 29-46 (2007).
58. Plotnikov, S.V., Sabass, B., Schwarz, U.S. & Waterman, C.M. High-resolution traction force microscopy. *Methods Cell Biol* **123**, 367-394 (2014).
59. Schindelin, J., Rueden, C.T., Hiner, M.C. & Eliceiri, K.W. The ImageJ ecosystem: An open platform for biomedical image analysis. *Mol Reprod Dev* **82**, 518-529 (2015).
60. Bolte, S. & Cordelieres, F.P. A guided tour into subcellular colocalization analysis in light microscopy. *J Microsc* **224**, 213-232 (2006).

61. Van Der Spoel, D. *et al.* GROMACS: fast, flexible, and free. *J Comput Chem* **26**, 1701-1718 (2005).
62. Bjelkmar, P., Larsson, P., Cuendet, M.A., Hess, B. & Lindahl, E. Implementation of the CHARMM Force Field in GROMACS: Analysis of Protein Stability Effects from Correction Maps, Virtual Interaction Sites, and Water Models. *J Chem Theory Comput* **6**, 459-466 (2010).
63. Jorgensen, W.L. & Madura, J.D. Quantum and statistical mechanical studies of liquids. 25. Solvation and conformation of methanol in water. *Journal of the American Chemical Society* **105**, 1407-1413 (1983).
64. Berendsen, H.J.C., Postma, J.P.M., Gunsteren, W.F.v., DiNola, A. & Haak, J.R. Molecular dynamics with coupling to an external bath. *The Journal of Chemical Physics* **81**, 3684-3690 (1984).
65. Bussi, G., Donadio, D. & Parrinello, M. Canonical sampling through velocity rescaling. *J Chem Phys* **126**, 014101 (2007).